ACS APPLIED MATERIALS & INTERFACES

Research Article

www.acsami.org

Fast Synthesis and Size Control of Gibbsite Nanoplatelets, Their Pseudomorphic Dehydroxylation, and Efficient Dye Adsorption

Seifeddine Louaer, Yao Wang,* and Lin Guo*

Key Laboratory of Bio-Inspired Smart Interfacial Science and Technology of Ministry of Education, School of Chemistry and Environment, Beihang University, Beijing, 100191, P. R. China

Supporting Information

ABSTRACT: In this paper, a simple and fast (4 days) procedure to synthesize colloidal gibbsite nanoplatelets (NPTs) from a single aluminum alkoxide (aluminum *sec*-butoxide) as precursor is presented. The introduction of a preheating step accelerated the precursor's hydrolysis/peptization and considerably shortened the overall reaction time while the acid concentration affected the uniformity of the platelets shape. This procedure was successfully exploited to rapidly produce gibbsite platelets of controllable sizes by combination with the seeded growth method. The use of a single alkoxide precursor induced high growth rates and allowed a fast control of the platelets size over a wide range (nano- to microscale after only three growth steps). No signs for size limitation were observed. The dehydroxylation sequence of the as-synthesized NPTs was systematically investigated. Thermally stable chi-alumina NPTs, pseudomorphs of the parent gibbsite platelets, with a micro/mesoporous structure and high specific surface area, were obtained. The synthesized gibbsite NPTs can efficiently adsorb Methyl Orange dye in wastewater treatment with removal efficiency up to 94.8%.

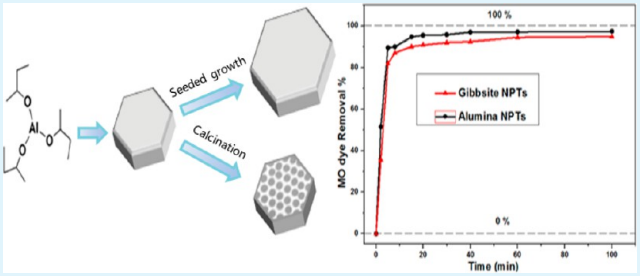

KEYWORDS: *gibbsite nanoplatelets, size control, seeded growth, pseudomorphic dehydroxylation, high surface area, MO dye removal*

INTRODUCTION

The synthesis of gibbsite (γ-Al(OH)$_3$) nanoparticles is of particular interest due to their numerous applicability as adsorbent,[1,2] fire-retardant,[3] polishing agent in toothpaste,[4] filler in paper manufacturing,[5] adjuvant for formulation of vaccine,[6] and as model system for the study of liquid crystal dynamics in the case of colloidal gibbsite nanoplatelets.[7−11] Moreover, gibbsite is a universal starting material for the fabrication of all alumina phases,[12] in their turn having a wide range of applications,[13,14] and since gibbsite-alumina transformation is pseudomorphic (i.e., the initial shape of gibbsite is kept),[12,15] controlled synthesis of gibbsite particles to predetermined shapes and sizes theoretically lead to a controlled-shape/size synthesis of alumina particles in all phases.

Industrially, gibbsite is extracted and purified by the Bayer process, a large-scale technique for the production of aluminum and alumina.[16,17] The gibbsite particles thus produced adopt nonregular morphologies with sizes ranging from several and up to hundreds of micrometers[18−20] which restricts their applicability. In the laboratory, several methods have been developed to synthesize nanosized gibbsite particles.[21−33] Among them, only few can achieve regularly shaped pure gibbsite nanoparticles.[24,27,28,30] Moreover, they all suffer from slow course which requires several days to weeks until gibbsite is completely crystallized.

It is known that for most applications the use of nanosized particles with controlled size and morphology is preferred to improve efficiency and/or enable better properties control. Because of the lack in fast procedures to synthesize regularly shaped pure gibbsite nanoparticles and the need to produce the industrially important various alumina phases with controlled morphology, the development of a new, simple, and fast method for the synthesis of gibbsite nanoparticles is of great interest.

Comparing to the aluminum salts precursors, the alkoxide route is advantageous for the higher stability of particles and the absence of destabilizing ions.[7,24] In general, the formation of gibbsite particles from thermal treatment of aluminum alkoxide(s) can be divided into two steps: (1) Hydrolysis and peptization of the alkoxide(s) to obtain a clear sol in presence of excess water and catalyzed by acid addition. (2) Then gibbsite crystallization under mild thermal conditions (≤100 °C). In the later step, a minimum of 3 days was found to be necessary to complete the crystallization. Thus, operating on the hydrolysis/peptization step is the key to shorten the overall reaction time.

In the present work, a facile procedure to synthesize monodispersed pseudohexagonal gibbsite nanoplatelets (NPTs) by a simple thermal treatment of one single aluminum alkoxide precursor is presented. Comparing to the frequently used method,[24] where a long stirring step (7−10 days at room

Received: July 5, 2013
Accepted: September 4, 2013
Published: September 4, 2013

temperature) of a mixture of two different aluminum alkoxides (aluminum isopropoxide + aluminum *sec*-butoxide) is needed, the present procedure only uses a single precursor (aluminum *sec*-butoxide), and an intermediate preheating step was introduced to accelerate the precursor's hydrolysis/peptization (completed in 1 day). This preheating treatment (at 55 °C) was carefully chosen at temperatures lower than those at which crystallization is facilitated. Although formation of gibbsite particles from the hydrothermal treatment of aluminum *sec*-butoxide was observed before,[21,31,34] to our knowledge it has not been studied so far. The combination of this easy method to synthesize gibbsite NPTs with the seeded growth method allowed a rapid size-control over a wide range. In addition, these rapidly synthesized gibbsite NPTs' dehydroxylation sequence was examined and their adsorption ability for removal of Methyl Orange (MO) dye was compared to that of porous alumina NPTs with high surface area.

EXPERIMENTAL SECTION

Materials. Aluminum *sec*-butoxide (ASB, ≥97%), and aluminum isopropoxide (AIP, ≥98%) were purchased from Alfa Aesar. Hydrochloric acid (HCl, 37%) was purchased from Beijing chemical works company (Beijing, China). All chemicals are of reagent grade and were used as received without further purification.

Synthesis of Gibbsite NPTs. In 500 mL of acidified aqueous solution with 0.02, 0.05, and 0.1 M HCl, were dissolved 0.08, 0.16, or 0.32 M ASB by vigorous stirring in a closed borosilicate container for 18 h at room temperature (25 ± 1 °C), followed by stirring for 6 h at 55 °C (preheating step) to accelerate the precursor's hydrolysis and peptization. The resulting solution was then heated without stirring at 85 °C for 72 h. After cooling to room temperature, the dispersion was washed by centrifugation-redispersion in water to remove any eventual unreacted precursor and/or dissolved byproducts, then stored in concentrated water solutions or recuperated and dried in oven at 60 °C overnight for subsequent calcination/characterization. Scheme1 shows a flowchart of the used procedure.

Scheme 1. Flow Chart for Synthesizing Platy-Shaped Gibbsite and Alumina Nanoparticles

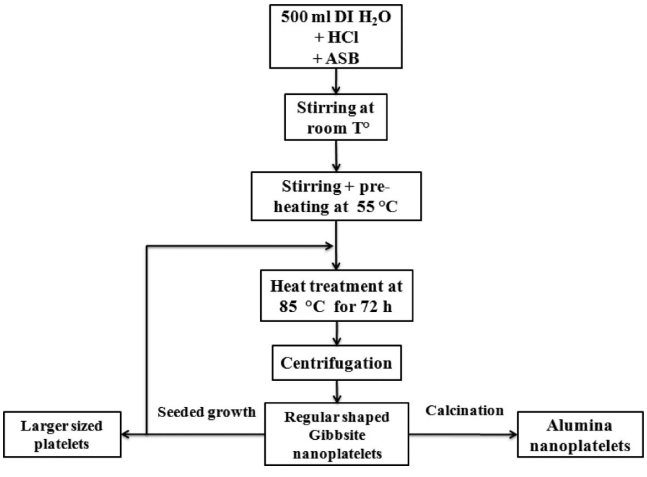

Size Controlled Synthesis of Gibbsite NPTs. Seeded growth was applied to the above-described method to obtain larger sized gibbsite platelets as described in ref 27. One half to two-third of the produced NPTs from each step are used as seeds for further growth. The seeds are added to a fresh solution of dissolved ASB (same concentrations), then heated at 85 °C under vigorous stirring to prevent sedimentation and secondary nucleation.

Calcination. Powdered samples were calcined in air for the whole temperature range from 100 to 1100 °C, with a heating rate of 10 °C/min, and a holding time of 1h at the desired temperature.

Dye Adsorption Experiment. The tests were carried out by dispersing 0.2 g of dried powdered samples in 50 mL of a 50 mg/L MO dye solution under stirring for a certain contact time. The pH of the solution was adjusted by addition of 0.1 M HCl or NaOH solution. An aliquot of the mixture solution was taken out at different time intervals. After centrifugation, the dye concentrations were measured in the supernatant part by UV−vis spectrophotometery.

Characterization. The morphology of the gibbsite NPTs was investigated by transmission electron microscopy (TEM) on a JEOL JEM-2100 microscope and atomic force microscopy (AFM) with a Bruker (Veeco) Dimension Icon instrument. Powder X-ray diffraction (XRD) was performed using a Rigaku D/max2200 X-ray diffractometer with Cu Kα (λ = 1.5406 Å) radiation scanned from 15° to 70°. In situ XRD was used to study the phase transformation during heating of gibbsite samples on a Shimadzu XRD-6000 instrument. Cu Kα (λ = 1.5406 Å) radiation scanned from 15° to 60° was also used. Thermogravimetric analysis (TGA) was carried out in air with an STA 449 F3 Jupiter (NETZSCH) analyzer between 40 and 1000 °C with a heating rate of 10 °C/min. BET surface area, pore volumes, and BJH pore size distributions measurements were carried out on a NOVA 2200e analyzer. The pore volumes were determined at a relative pressure (P/P_0) of 0.970. Before analysis, the first three samples (as-synthesized gibbsite, the 200 and 300 °C calcined samples) were degassed at 100, 150, and 200 °C, respectively, while for the rest of the samples degassing was performed at 300 °C for 4 h.

RESULTS AND DISCUSSION

Screening the Best Conditions to Synthesize Gibbsite NPTs. In order to find the optimum conditions to obtain uniformly shaped gibbsite NPTs with the shorter reaction time, a series of tests were conducted by varying the starting acid and precursor's concentrations. The details of the adopted reaction conditions are shown in Table 1.

As previously reported,[34] we observed that the acidity of the medium had an effect on both hydrolysis/peptization and crystallization steps. In general, the hydrolysis and peptization completion depended on the molar ratio of Al to H^+. Indeed, at high Al to H^+ molar ratio (ASB2 and ASB4 samples), the added ASB precursor did not completely dissolve after the 6 h of preheating step which was enough for the samples with lower Al to H^+ molar ratio (ASB1 and ASB3) to turn into a very clear sol. Thus, the concentrations of ASB3 sample were selected to achieve shorter reaction time and higher NPTs yield.

Concerning crystallization, the three samples ASB1, ASB3 and ASB5 were selected to investigate the effect of HCl concentration on the particles shape. Typical TEM images of the as synthesized samples are presented in Figure 1. The particles shape was clearly affected by the acidity of the medium. At acid concentration of 0.02 M (ASB1), various platy shapes (lozenges, truncated lozenges, truncated triangles and hexagons) with large difference in sizes were observed (Figure 1a), while in the 0.05 M HCl acidified sample (ASB3) well-shaped, fairly monodisperse pseudohexagonal NPTs, with average diameter of ∼240 nm and thickness of ∼10 nm were obtained (Figure 1b). The inset selected area electron diffraction (SAED) pattern confirms their single-crystalline structure. For the 0.1 M HCl acidified sample (ASB5), the TEM images revealed platelets with irregularly rounded edges (Figure 1c), likely resulting from the dissolution of well-shaped hexagonal gibbsite platelets due to the high acidity,[35] which may also explains the decrease in its XRD peaks intensity. All

Table 1. Details of Reaction Conditions, Resulting Sols, Total Reaction Time, and Shape Uniformity

samples	[ASB] (mol/L)	[HCl] (mol/L)	stirring time at rt	preheating time[a]	complete dissolution	heating time (at 85 °C)	total reaction time	shape uniformity
ASB1	0.08	0.02	18 h	6 h	yes	72 h	4 days	no
ASB2	0.16	0.02	18 h	6 h	no			
ASB3	0.16	0.05	18 h	6 h	yes	72 h	4 days	yes
ASB4	0.32	0.05	18 h	6 h	no			
ASB5	0.16	0.1	18 h	6 h	yes	72 h	4 days	no

[a]Stirring and heating at 55 °C.

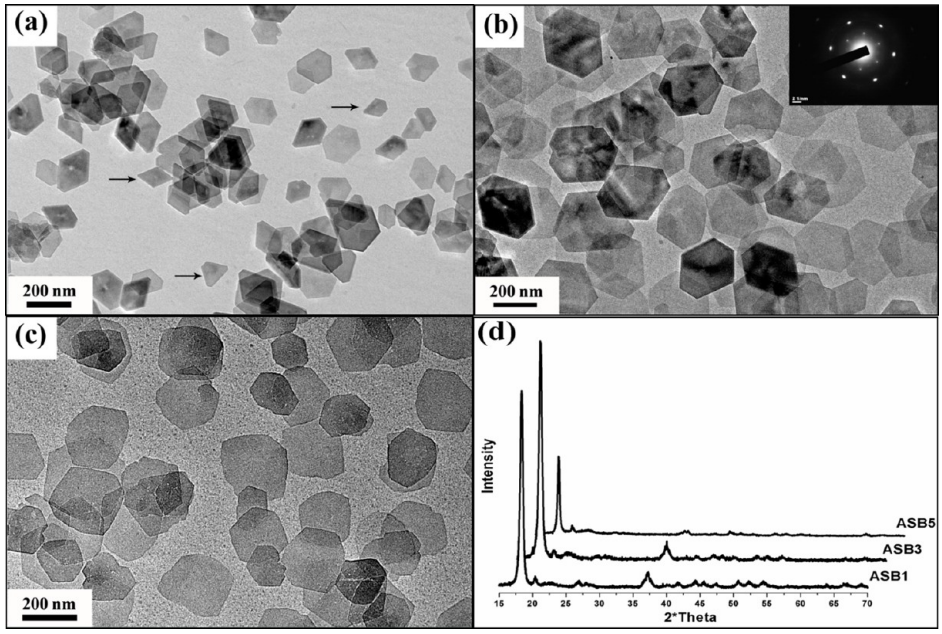

Figure 1. Morphologies obtained at different acid (HCl) concentrations: (a) 0.02 M (arrows showing the various morphologies), (b) 0.05 M (inset: SAED pattern indicating the NPTs are single-crystal), and (c) 0.1 M. (d) XRD patterns of the former products.

the samples' XRD profiles (Figure 1d) were identified to the monoclinic gibbsite (JCPDS PDF no. 74-1775).

The chemical reactions involved in the formation of the gibbsite structure from ASB as single molecular precursor can be divided into two steps: complete dissolution of the precursor and crystallization.

After the hydrolysis (reaction 1) and peptization are completed (clear sol), and driven by increasing the temperature, crystallization into gibbsite occurs in acidic conditions by arrangement of the $Al(OH)_3$ entities into a layered structure, where each layer consists of a double layer of closed packed OH ions, with Al^{3+} cations occupying two-thirds of the octahedral cavities and the different layers are hold together by interlayer hydrogen bonds.[36]

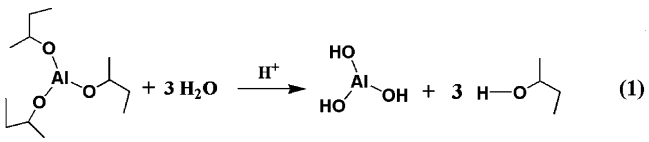

(1)

Since the lozenge shape is accepted to be the basic morphology for gibbsite crystals,[18,37] it was perceived that all the observed shapes can be thus derived as shown in Figure 2. The lozenge shape was truncated by the development of (100) facets at different rates, influenced by the acid concentration, leading to the observed truncated lozenge, truncated triangle and hexagonal platelet shapes. The uniform hexagonal shape was favored at relatively high acidity (0.05 M).

The application of this new procedure to aluminum isopropoxide (AIP) as a single alkoxide precursor was also investigated. Even at low Al to H^+ molar ratio, the AIP was found to need a long preheating time to be completely dissolved. Also, after thermal treatment at 85 °C for 72 h, the resulting colloid showed the presence of two particles types: highly polydisperse gibbsite NPTs along with amorphous needlelike particles (Figure S1, Supporting Information).

Size Controlled Synthesis of Gibbsite NPTs. Larger sized gibbsite platelets were easily obtained by combining the presented fast synthesis method with the well-established seeded growth procedure. Figure 3 shows TEM images of gibbsite platelets after one (a) and three (b) additional growth steps. Highly monodispersed pseudohexagonal NPTs with ~511 nm diameter and ~20 nm in thickness were obtained for the first growth step. Moreover, the NPTs were able to reach the micrometer scale (~1 μm diameter and ~30 nm thickness) after two more growth steps. The pseudohexagonal shape was kept, and some platelets exhibited a tendency to align on each other. Also, the SAED pattern still shows a single-crystalline structure even after the third growth step, which indicates that the seeded growth is epitaxial, as suggested in previous works.[27]

Table 2 shows the evolution of the platelets sizes for all growth steps. A change in the aspect ratio of the platelets was

dx.doi.org/10.1021/am402677v | ACS Appl. Mater. Interfaces 2013, 5, 9648−9655

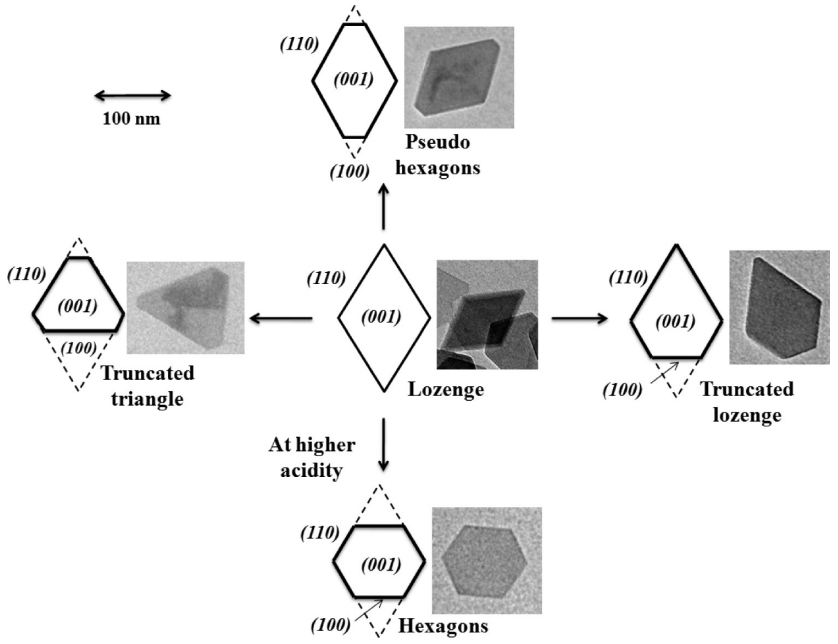

Figure 2. Obtained morphologies of gibbsite crystals grown from ASB precursor and their growth relationship to the lozenge shape.

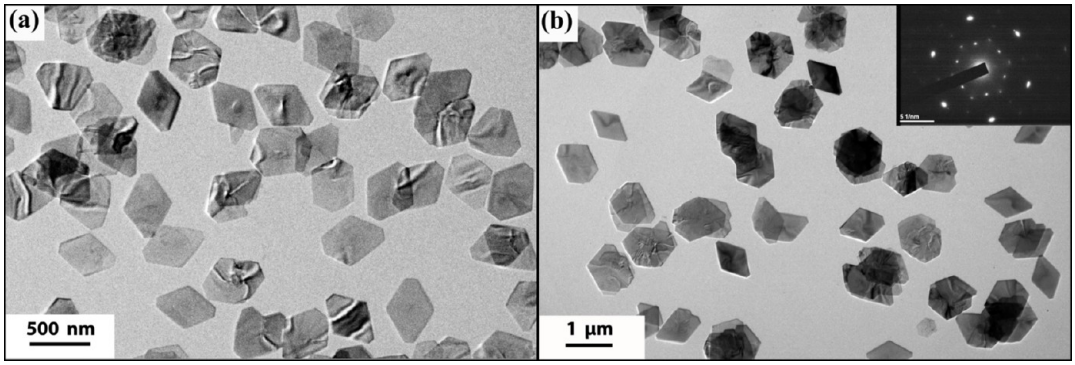

Figure 3. TEM of larger sized gibbsite platelets obtained by seeded growth (a) after one growth step (size: ~510 nm) and (b) after three growth steps (size: ~1 μm). Inset: SAED pattern indicating the platelets are still single-crystal.

Table 2. Size Evolution during Seeded Growth and the Corresponding Aspect Ratios

growth step	diameter (TEM)	thickness (AFM)	aspect ratio
step 0 (seeds)	240 nm ± 13%	10 nm ± 20%	24
step 1	511 nm ± 5%	20 nm ± 11%	25.5
step 2	710 nm ± 5%	25 nm ± 9%	28.4
step 3	1.004 μm ± 7%	30 nm ± 12%	33.3

observed. It means different crystal planes had different growth rates, a known growth habit for gibbsite crystals.[18,27]

The combination of the new method to synthesize gibbsite NPTs with seeded growth accentuated its fastness advantage and considerably shortened the overall reaction time as compared to the frequently adopted method.[24,27] Indeed, using the literature procedure, at least four additional growth steps with a total reaction time of 5 × 13 days are needed to reach a platelets size of 500 nm.[27] In the present method, one seeded growth step was sufficient to reach the same size range, which only requires 2 × 4 days in total. Moreover, the platelets reached the micrometer scale (~1 μm) simply after three growth steps (4 × 4 days). This relatively fast growth rate (≥200 nm per growth step) is attributed to the use of a single aluminum alkoxide (ASB) as precursor, which allows higher homogeneity and more growth stability. Finally, except the need of vigorous stirring to avoid sedimentation of the seeds when growing, there were no signs for size limitation. It is believed that further growth would lead to even bigger platelets.

Gibbsite NPTs Dehydroxylation Sequence. Since the transformation of gibbsite to alumina is generally pseudomorphic,[12,15] and since gibbsite is a common precursor to all alumina phases,[12,38] it is interesting to investigate the morphology and decomposition sequence of the resulting alumina derived from the newly synthesized gibbsite NPTs. Due to their fast reaction time, regular shape, and monodispersity, gibbsite NPTs synthesized according to the optimized reaction conditions of sample ASB3 were used throughout the following experiments.

Gibbsite dehydroxylation was first examined by thermal gravimetric analysis (TGA). Figure 4 shows the TGA curve of the studied sample. A steep weight loss between 270 and 400 °C due to fast water elimination is first noted, and then the weight continues decreasing slowly until 1000 °C. The final weight loss of ~35% is in accord with the gibbsite one. This value is similar to the theoretical one (34.6%), calculated from gibbsite decomposition according to the reaction:

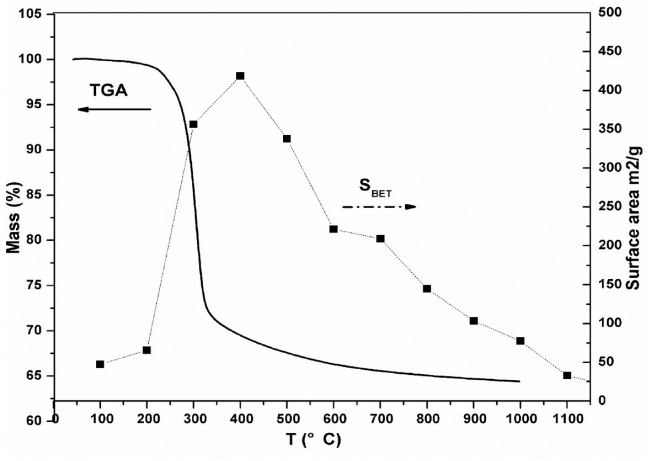

Figure 4. Gibbsite TGA curve and surface area evolution with calcination temperature.

$$2Al(OH)_3 \rightarrow Al_2O_3 + 3H_2O$$

The nature of the formed alumina phases and their transition sequence was followed by in situ X-ray diffraction and the results are shown in Figure 5. At 200 °C, the gibbsite phase was still predominant with a decrease in the peaks intensity recorded comparing to gibbsite sample dried at 100 °C. This is due to thermal decomposition initiation. Starting from 300 °C, gibbsite peaks completely disappeared, leaving place to chi-alumina phase. This chi-alumina phase was found to be thermally stable even at temperatures as high as 1000 °C, after which a direct transformation to pure alpha-alumina was observed at relatively low temperature (1100 °C). To examine the phase transformation between 1000 and 1100 °C more closely, additional XRD measurements at 1050 °C was performed. A very unstable kappa-phase was observed at 1050 °C which quickly disappears after slight increase in temperature to 1100 °C, leaving place to the thermodynamically stable alpha-alumina phase.

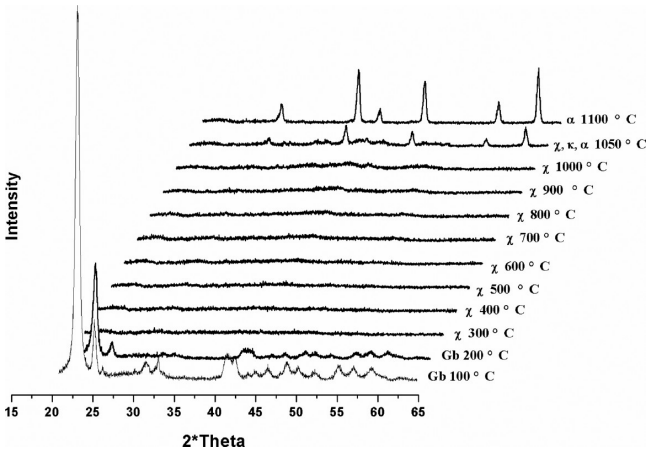

Figure 5. In situ XRD patterns of calcined gibbsite samples showing the phase transition at different temperatures.

The morphology and microstructure of the calcined samples were investigated by TEM (Figure 6). Most of the produced alumina nanoparticles kept the initial gibbsite hexagonal platy shape until temperatures as high as 900 °C (Figure 6a–f), after which the platelet shape was lost due to crystallites growth to larger sizes (Figure 6g). This shape conservation is known as pseudomorphic transformation, and is a known process for gibbsite.[15]

If the external platelet shape of the starting aluminum hydroxide was maintained during conversion to the oxide state, only the development of a pore structure inside the platelets and the increase in density can explain the significant weight loss (~35%) accompanying alumina formation. This porous structure was revealed by TEM. From Figure 6, it can be seen that there was an evolution in pore and crystallite's sizes with increasing the calcination temperatures. Crystallites sizes calculated from TEM images are shown in Table 3. A continuous increase in chi-alumina crystallites size was observed during the calcination cycle until it reaches a critical size between 1000 and 1100 °C where the next alumina phase nucleation occurs. High resolution TEM image (Figure S3, Supporting Information) of the 700 °C calcined sample reveals that interconnected nanodomains (crystallites) with size of about ~6 nm have a preferential orientation which resulted in a single-crystal-like SAED pattern. In addition, the HRTEM image shows that the pores between these crystallites are not uniformly ordered and are unlikely to be connected into a 3D-network.

Table 3 also shows the evolution of the surface area with respect to calcination temperature. The surface area increased

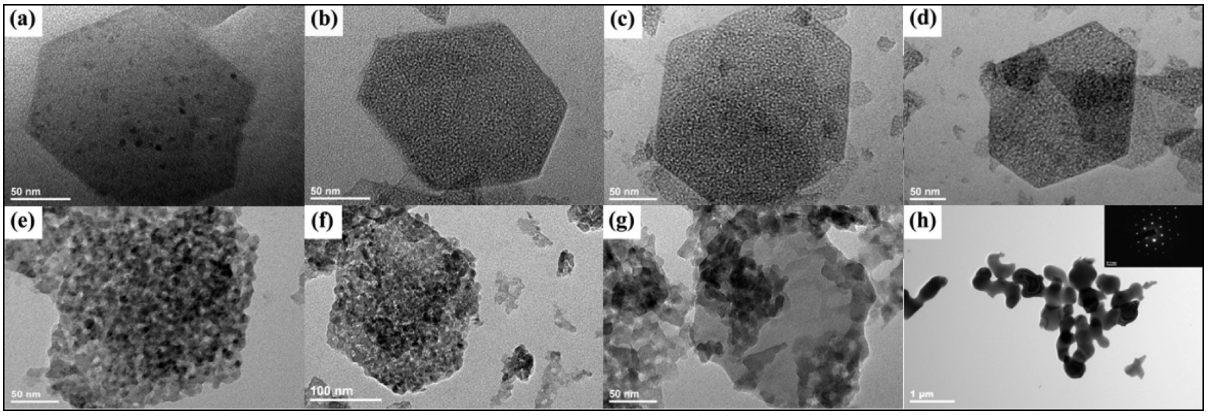

Figure 6. TEM images of the gibbsite samples calcined at (a) 200 °C, (b) 300 °C, (c) 400 °C, (d) 500 °C, (e) 700 °C, (f) 900 °C, (g) 1000 °C, and (h) 1100 °C, showing the platelet shape remaining and the development of a porous structure (the inset is the corresponding SAED pattern).

Table 3. Surface area, Pore Volume, Pore Size, and Crystallite Size of the Different Samples

calcination T (°C)	S_{BET} (m^2/g)	pore volume (cm^3/g)	pore size (nm)[a]	Crystallite Size (nm)[b]	material/phase
100	47.37	0.17	13.96		gibbsite
200	65.66	0.21	12.54		gibbsite
300	356.45	0.41	0.91 and 15.43	1.5	chi-alumina
400	418.55	0.45	0.92 and 13.39	2.8	chi-alumina
500	337.74	0.458	1.70 and 13.45	4.0	chi-alumina
600	221.16	0.44	3.44 and 15.88		chi-alumina
700	208.86	0.46	2.98 and 13.50	6.4	chi-alumina
800	144.87	0.35	3.80 and 15.88		chi-alumina
900	103.45	0.42	4.97 and 16.96	8.8	chi-alumina
1000	77.4	0.40	22.69	15.4	chi-alumina
1100	33.12	0.093	22.12		alpha-alumina

[a]From BJH method. [b]From TEM.

quickly to reach a maximum value of 418 m^2/g recorded at the particular temperature of 400 °C, after which it starts to decrease gradually. Exceptionally, the samples still show a high surface area (>100 m^2/g), even at temperatures as high as 900 °C. From Figure 4, we can see that the maximum surface area at 400 °C corresponds to the end of the main weight loss due to water elimination. For the first three porous samples (i.e., at 300, 400, and 500 °C), the development of micropores with diameters less than 2 nm (Figure S4, Supporting Information) may explain their highest surface area values (356, 418, and 337 m^2/g, respectively). The secondary pores with sizes bigger than 10 nm are likely from platelets stacking which lead to formation of slit-like pores since these pores also show up in the nonporous gibbsite sample with no heat treatment (at 100 °C) and in the alpha-alumina with smooth surface (at 1100 °C).

A close inspection of the adsorption/desorption isotherms shapes (Figure S5, Supporting Information) reveals that, from 300 to 800 °C, the samples exhibited type IV adsorption/desorption isotherms, while the first two (at 100 and 200 °C) and the last three (from 900 to 1100 °C) samples had type V isotherms, with all samples exhibiting a hysteresis loop at high relative pressures, a typical feature associated with capillary condensation within mesopores. Type IV isotherms are characteristic of a multilayer adsorption while type V indicates a weak adsorbent–adsorbate interactions comparing to the adsorbate–adsorbate ones.[39] This difference in adsorption behavior between the different calcined samples suggests a difference in their external surface chemistry. The absence of coordinatively unsaturated Al^{3+} sites (which appears due to water elimination) in non-heat-treated gibbsite samples and their disappearance at high temperatures (become coordinatively saturated due to atoms rearrangement during phase transformation to the stable alpha-alumina) may explain the weaker adsorbent–adsorbate interactions and plays an important role in the adsorption mechanism. In addition, all the samples showed a hysteresis loop shape of H3 type, usually observed for aggregates of platelike particles and leads to formation of slit-shaped pores,[39] which justifies the presence of the secondary pores (>10 nm) observed in all samples.

Application for MO Dye Adsorption. Various kinds of organic dyes appear in the sewage of many industries such as textiles, leather, paper, plastics, cosmetics, and so forth.[40] Since the public perception of water quality is greatly influenced by its appearance, color is the first contaminant to be recognized in water and removal of color from wastewater is one of the challenging problems in the field of environmental chemistry.[41,42]

Promoted by their surface chemistry, the obtained NPTs can make good adsorbents for wastewater treatment. Thus, investigations for removal of Methyl Orange dye as model contaminant were carried out.

Figure 7 displays MO removal capacities of the samples calcined at different temperatures. The result shows that the

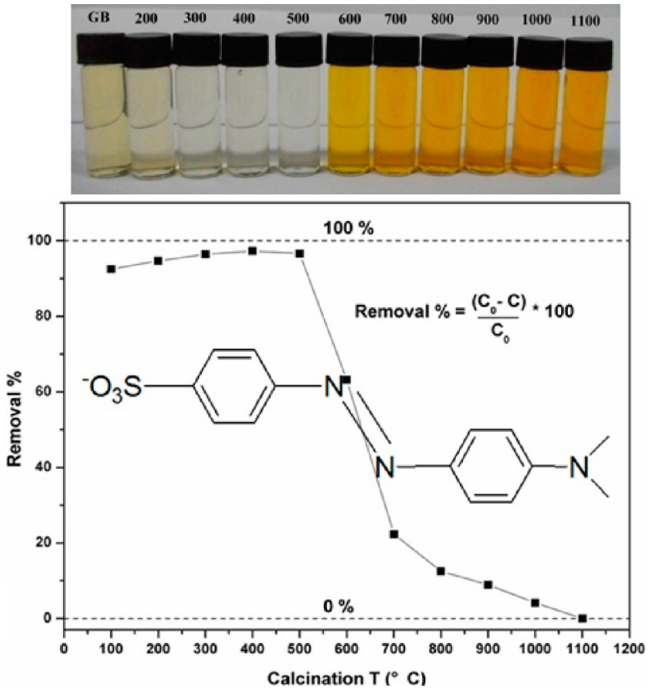

Figure 7. Evolution of MO dye removal with calcination temperatures: top, photographs; bottom, removal % and MO molecular structure. Tests were carried out after a contact time of 40 min at pH = 5.7.

maximum removal abilities of 96.4%, 97.3%, and 96.7% were recorded for the samples possessing the maximum surface areas (i.e., at 300, 400, and 500 °C calcined samples, respectively). Surprisingly, despite their low specific surface area, the as-synthesized gibbsite platelets and the 200 °C-calcined samples exhibited removal abilities (92.5% and 94.7% respectively) comparable to those of samples with high surface area. This means the MO dye adsorption on the two sample categories (gibbsite surface with low specific surface area and alumina surface with high specific surface area) involves different adsorption mechanisms. After the calcination temperature of

500 °C, a fast decrease in dye removal capacity was recorded until 1100 °C, where no dye adsorption was observed.

For comparison and to understand the adsorption mechanisms on the two different sample categories, the as-synthesized gibbsite sample and the 400 °C calcined sample were chosen to study the adsorption of Methyl Orange at various pH and the results are given in Figure 8.

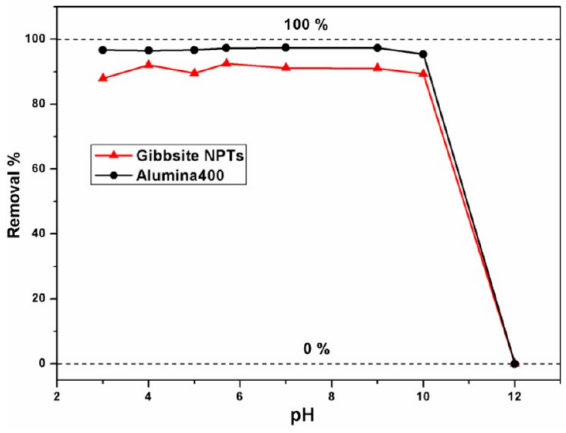

Figure 8. Effect of the initial pH value on MO dye uptake by the as-synthesized gibbsite and 400 °C calcined (Alumina400) samples. Tests were carried out after a contact time of 40 min.

In the pH range of 3−10, a high uptake was recorded for both samples. At such pH conditions, the gibbsite surface is positively charged (gibbsite isoelectric point ≥ 10)[24,43] and electrostatic attraction with negatively charged group ($-SO_3^-$) of MO likely takes place. For the calcined sample, the interaction probably occurs between the $-SO_3^-$ group and some specific sites (Al^{3+} Lewis acid sites), apparently not present on the entire surface of the adsorbent.[44] However, at higher pH values (pH = 12), no dye adsorption was observed in both samples. For gibbsite, the change in surface charge from positive to negative above its isoelectric point results in an electrostatic repulsion between the adsorbent surface and adsorbate molecules and thus in loss of dye uptake ability. In the case of calcined sample, the absence of MO sorption at high pH values might be due to shielding of the acid sites on alumina surface by OH^- ions.[44]

The evolution of Methyl Orange removal with contact time in Figure 9 shows that the curves are of saturation type with a fast initial adsorption rates which rapidly reach an equilibrium value, suggesting a possible monolayer coverage of dyes on the surface of the adsorbent.[45]

To investigate the sorption kinetics, adsorption data are analyzed according to two kinetic models, pseudo-first-order (PFO) and pseudo-second-order (PSO).[46] The best model is selected based on the linear regression coefficient R^2 values. The fitting results (Figure S6 and Figure S7, Supporting Information) show that adsorption of MO dye on both adsorbent categories fits better to the pseudo-second-order model ($R^2 > 0.999$) with k_2 constants of 5.57×10^{-2} and 1.008×10^{-1} g·mg^{-1}·min^{-1} for gibbsite and 400 °C calcined samples, respectively.

CONCLUSIONS

In summary, a simple and fast procedure to synthesize pseudohexagonal gibbsite NPTs by thermal treatment of one single aluminum alkoxide as precursor was presented. The acidity of the medium affected the NPTs shape uniformity. Monodisperse and uniform hexagonal shape was favored at acid concentrations higher than 0.02 M.

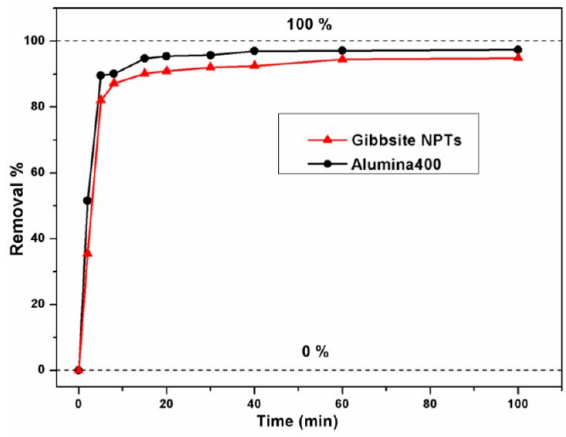

Figure 9. Adsorption data for removal of MO versus contact time for the as-synthesized gibbsite and the 400 °C calcined (Alumina400) samples.

Combination of this new method to synthesize gibbsite NPTs with seeded growth repeatedly resulted in a rapid control over the platelets size and considerably shortened the overall reaction time. The higher homogeneity and growth stability, generated from the use of a single aluminum alkoxide, led to fast growth rates per step and allowed controlling the size of the platelets over a wide sizes range. The microscopic characterization showed that this seeded growth was both anisotropic and epitaxial. Moreover, no signs for size limitations were observed.

The thermal decomposition of the as-synthesized gibbsite NPTs was pseudomorphic and resulted in thermally stable chi-alumina platelets with a micro/mesoporous structure and high specific surface area.

At room temperature and over a wide pH range, the obtained gibbsite NPTs showed a good ability for Methyl Orange dye removal comparable to that of porous alumina with high surface. Other eminent applications would be use for the study of liquid crystals phase behavior (controlled-size gibbsite NPTs) and as catalysts support (porous alumina NPTs).

ASSOCIATED CONTENT

Supporting Information

Details on the adopted procedure tested with AIP as single precursor and the corresponding TEM and XRD results along with HRTEM image, pore-size distributions, nitrogen adsorption/desorption isotherms of the studied samples, plus dye sorption data fitting to pseudo-first- and second-order kinetic models. This material is available free of charge via the Internet at http://pubs.acs.org.

AUTHOR INFORMATION

Corresponding Authors

*E-mail: yao@buaa.edu.cn.
*E-mail: guolin@buaa.edu.cn.

Notes

The authors declare no competing financial interest.

■ ACKNOWLEDGMENTS

This work was supported by: the Project of Major National Basic Research Development Program (2010CB934700), Program for New Century Excellent Talents in University (NCET-10-0035), National Natural Science Foundation of China (51073006, 51373005), PhD Programs Foundation of Ministry of Education of China (20101102120043), and the Fundamental Research Funds for the Central Universities.

■ REFERENCES

(1) Goldberg, S. *Soil Sci.* **2010**, *175*, 105−110.
(2) Huittinen, N.; Rabung, T.; Lützenkirchen, J.; Mitchell, S. C.; Bickmore, B. R.; Lehto, J.; Geckeis, H. *J. Colloid Interface Sci.* **2009**, *332*, 158−164.
(3) Yen, Y.-Y.; Wang, H.-T.; Guo, W.-J. *J. Appl. Polym. Sci.* **2013**, *130*, 2042−2048.
(4) Mori, S.; Nakajima, T. U.S. patent, No 6,113,887, Sep. 5, 2000.
(5) Maus, T. U.S. patent, No US 2010/0175844 A1, Jul. 15, 2010.
(6) Ulanova, M.; Tarkowski, A.; Hahn-Zoric, M.; Hanson, L. Å. *Infect. Immun.* **2001**, *69*, 1151−1159.
(7) Van der Kooij, F. M.; Lekkerkerker, H. N. W. *J. Phys. Chem. B* **1998**, *102*, 7829−7832.
(8) Van der Kooij, F. M.; Kassapidou, K.; Lekkerkerker, H. N. W. *Nature* **2000**, *406*, 868−871.
(9) Verhoeff, A. A.; Wensink, H. H.; Vis, M.; Jackson, G.; Lekkerkerker, H. N. W. *J. Phys. Chem. B* **2009**, *113*, 13476−13484.
(10) Kleshchanok, D.; Meijer, J.-M.; Petukhov, A. V.; Portale, G.; Lekkerkerker, H. N. W. *Soft Matter* **2011**, *7*, 2832−2840.
(11) Wijnhoven, J. E. G. J.; van't Zand, D. D.; van der Beek, D.; Lekkerkerker, H. N. W. *Langmuir* **2005**, *21*, 10422−10427.
(12) Santos, P. S.; Santos, H. S.; Toledo, S. P. *Mater. Res.* **2000**, *3*, 104−114.
(13) Grant, S. M.; Woods, S. M.; Gericke, A.; Jaroniec, M. *ACS Appl. Mater. Interfaces* **2011**, *3*, 4480−4486.
(14) Materna, K. L.; Grant, S. M.; Jaroniec, M. *ACS Appl. Mater. Interfaces* **2012**, *4*, 3738−3744.
(15) Yen, F.-S.; Cheng, P.-L.; Huang, H.-Y.; Lin, T.-C. *J. Am. Ceram. Soc.* **2009**, *92*, 2089−2092.
(16) Hind, A. R.; Bhargava, S. K.; Grocott, S. C. *Colloids Surf., A* **1999**, *146*, 359−374.
(17) Whittington, B.; Ilievski, D. *Chem. Eng. J.* **2004**, *98*, 89−97.
(18) Sweegers, C.; de Coninck, H. C.; Meekes, H.; van Enckevort, W. J. P.; Hiralal, I. D. K.; Rijkeboer, A. *J. Cryst. Growth* **2001**, *233*, 567−582.
(19) Sweegers, C.; van Enckevort, W. J. P.; Meekes, H.; Bennema, P.; Hiralal, I. D. K.; Rijkeboer, A. *J. Cryst. Growth* **1999**, *197*, 244−253.
(20) Cesteros, Y.; Salagre, P.; Medina, F.; Sueiras, J. E. *Chem. Mater.* **2001**, *13*, 2595−2600.
(21) Philipse, A. P.; Nechifor, A.-M.; Patmamanoharan, C. *Langmuir* **1994**, *10*, 4451−4458.
(22) Liu, Y.; Ma, D.; Blackley, R. A.; Zhou, W.; Han, X.; Bao, X. J. *J. Phys. Chem. C* **2008**, *112*, 4124−4128.
(23) Lee, Y.-P.; Liu, Y.-H.; Yeh, C.-S. *Phys. Chem. Chem. Phys.* **1999**, *1*, 4681−4686.
(24) Wierenga, A. M.; Lenstra, T. A. J.; Philipse, A. P. *Colloids Surf., A* **1998**, *134*, 359−371.
(25) Rasmussen, D. H.; Brancewicz, C.; Das, B.; Graeffe, M.; Rosenholm, J.; Toscano, A. *J. Dispersion Sci. Technol.* **2001**, *22*, 491−498.
(26) Phambu, N.; Humbert, B.; Burneau, A. *Langmuir* **2000**, *16*, 6200−6207.
(27) Judith E.G.J, W. *J. Colloid Interface Sci.* **2005**, *292*, 403−409.
(28) Shen, S.; Chow, P. S.; Chen, F.; Feng, S.; Tan, R. B. H. *J. Cryst. Growth* **2006**, *292*, 136−142.
(29) Kumara, C. K.; Ng, W. J.; Bandara, A.; Weerasooriya, R. *J. Colloid Interface Sci.* **2010**, *352*, 252−258.
(30) Rosenqvist, J.; Persson, P.; Sjöberg, S. *Langmuir* **2002**, *18*, 4598−4604.
(31) Buining, P. A.; Pathmamanoharan, C.; Jansen, J. B. H.; Lekkerkerker, H. N. W. *J. Am. Ceram. Soc.* **1991**, *74*, 1303−1307.
(32) Vieira Coelho, A. C.; Souza Santos, H. d.; Kiyohara, P. K.; Marcos, K. N. P.; Souza Santos, P. d. *Mater. Res.* **2007**, *10*, 183−189.
(33) Wang, D.-G.; Guo, F.; Chen, J.-F.; Zhao, R.-H.; Zhang, Z.-T. *Mater. Chem. Phys.* **2008**, *107*, 426−430.
(34) Yoldas, B. E. *Am. Ceram. Soc. Bull.* **1975**, *54*, 289−291.
(35) Wijnhoven, J. E. G. J. *Chem. Mater.* **2004**, *16*, 3821−3828.
(36) Demichelis, R.; Civalleri, B.; Noel, Y.; Meyer, A.; Dovesi, R. *Chem. Phys. Lett.* **2008**, *465*, 220−225.
(37) Sweegers, C.; Plomp, M.; de Coninck, H. C.; Meekes, H.; van Enckevort, W. J. P.; Hiralal, I. D. K.; Rijkeboer, A. *Appl. Surf. Sci.* **2002**, *187*, 218−234.
(38) Wefers, K.; Misra, C. *Alcoa Technical Paper No. 19, Revised*; Alcoa Laboratories: Pittsburgh, PA, 1987; p 47.
(39) Sing, K. S. W. *Pure Appl. Chem.* **1985**, *57*, 603−619.
(40) Chiou, M.-S.; Ho, P.-Y.; Li, H.-Y. *Dyes Pigm.* **2004**, *60*, 69−84.
(41) Crini, G. *Bioresour. Technol.* **2006**, *97*, 1061−1085.
(42) Salem, I. A.; El-Maazawi, M. S. *Chemosphere* **2000**, *41*, 1173−1180.
(43) Adekola, F.; Fédoroff, M.; Geckeis, H.; Kupcik, T.; Lefèvre, G.; Lützenkirchen, J.; Plaschke, M.; Preocanin, T.; Rabung, T.; Schild, D. *J. Colloid Interface Sci.* **2011**, *354*, 306−317.
(44) Iida, Y.; Kozuka, T.; Tuziuti, T.; Yasui, K. *Ultrasonics* **2004**, *42*, 635−639.
(45) Annadurai, G.; Juang, R.-S.; Lee, D.-J. *J. Hazard. Mater.* **2002**, *92*, 263−274.
(46) Ho, Y.-S. *J. Hazard. Mater.* **2006**, *136*, 681−689.